journal

J. Am. Ceram. Soc., 93 [11] 3709–3719 (2010)
DOI: 10.1111/j.1551-2916.2010.03974.x

Growth of One-Dimensional Nanostructures in Porous Polymer-Derived Ceramics by Catalyst-Assisted Pyrolysis. Part II: Cobalt Catalyst

Cekdar Vakifahmetoglu and Paolo Colombo*,†,‡

Dipartimento di Ingegneria Meccanica—Settore Materiali, University of Padova, 35131 Padova, Italy

Sara Maria Carturan

Laboratori Nazionali di Legnaro, University of Padova & INFN, 35020 Legnaro, Padova, Italy

Eckhard Pippel and Jörg Woltersdorf

Max-Planck-Institut für Mikrostrukturphysik, D-06120 Halle, Germany

Via catalyst-assisted pyrolysis, Si_3N_4 and SiC nanowires were produced on the cell walls of polymer-derived ceramic foams. The pyrolysis atmosphere and temperature were the main parameters affecting their development: silicon nitride single-crystal nanowires formed under nitrogen, while silicon carbide ones were produced under argon, and their amount increased with the increasing pyrolysis temperature. Brunauer–Emmett–Teller analysis showed that the presence of the nanowires afforded high specific surface area (SSA) values to the macroporous ceramic foams, ranging from 10 to 110 m^2/g. Co-containing samples developed higher SSA values, especially after pyrolysis at 1400°C in N_2, than samples containing Fe as a catalyst. The differences were explained in terms of morphology (diameter and assemblage), which depended on the processing conditions and the catalyst type (Co or Fe).

I. Introduction

The porous component containing pores with dimension within two or more length scales is referred to as a material with hierarchical porosity. Different microstructures may exist according to the range of pore sizes that are involved in the porous structure, i.e. bimodal size distribution (micro-meso, meso-macro, and micro-macro), or trimodal (micro-meso-macro). Such components are of significant technological interest and are used in several industrial processes and household products. Applications include catalysis, filtration (of liquids or gases), extraction, separation, sorption, and scaffolds for biological applications.[1] In some instances, it is advantageous to have a component possessing a large (from several micrometers to a few millimeters) interconnected porosity. In fact, the macroporous ceramic framework offers chemical and mechanical stability, as well as high convective heat transfer, high turbulence, low pressure drop, and a high external mass transfer rate due to interconnections between the macropores.[2] The solid walls surrounding these pores can be modified to provide the functionality for a given application (such as chemical affinity toward specific pollutants, surface roughness, etc.). In particular, the presence of a high specific surface area (SSA) is greatly demanded to accelerate surface reactions due to enhanced interfacial contact area between the substrate and the active phase (gas or liquid phase), i.e. roughly speaking; the higher the SSA is, the higher the reactivity of the material.[3]

The presence of one-dimensional (1D) nanostructures (such as nanofibers/wires) on the surface of a dense material may lead to an increase of its SSA. In fact, their unique morphology (i.e., nanosize diameter, high aspect ratio, and presence of bundles and aggregates) provides significant additional geometric surface, and voids (pores) of various size (micro-, meso-, and macro-) can be found among the fibers and between the fibers and the host matrix. This feature has been exploited to transform low SSA cellular ceramics into moderate SSA materials, in which nanofibers/wires are obtained on the cell walls of the host ceramic via *in situ* formation,[4] therefore enabling it to fulfill similar applications to those of a properly termed hierarchical porosity component. Moreover, this approach enables to add alternative phases to the material, which can further functionalize the system (e.g., altering its mechanical, magnetic, or electrical properties). Both ceramic honeycombs and ceramic foams have been used as substrates on which different types of 1D nanostructures were created, using different approaches. These include carbon nanofibers (CNFs),[5–13] carbon nanotubes (CNTs),[14–20] or SiC nanofibers.[4,21] Previous works demonstrated that moderate (~ 30 m^2/g) to high (~ 150 m^2/g) values for the SSA could be obtained, depending on the amount, length, and diameter of the nanostructures.[4,12,21]

The release of decomposition gases, when pyrolyzing preceramic polymers at high temperature in inert atmosphere, has led some researchers to develop 1D nanostructures in the pores of the formed ceramics via catalyst-assisted pyrolysis (CAP), as discussed in the companion paper (Part I).[22–28] Using emulsion-based processing of a preceramic polymer-containing transition metals such as Fe, Co, Ni, or Pd, nanofibers consisting of β-SiC/α-SiO_2 were also very recently obtained in the pores of the produced SiOC foam.[29] An application of this processing concept to the growth of nanofibers on the surface of cellular polymer-derived ceramic has been recently pursued by Yoon *et al.*[30] and in our laboratory.[28,31] The first authors reported the formation of highly aligned macroporous SiC ceramics decorated with homogenously distributed SiC nanowires, produced by unidirectional freeze casting of SiC/camphene slurries with different amounts of the PCS precursor. Iron, an unwanted impurity in the starting SiC powder, was the catalyst enabling the growth of the nanowires, which afforded SSA values ranging from 30 to 86 m^2/g, depending on the length of the nanostructures. The work in our laboratory has focused on the deliberate one-pot

T. Parthasarathy—contributing editor

Manuscript No. 27428. Received January 21, 2010; approved June 9, 2010.
*Member, The American Ceramic Society.
†Author to whom correspondence should be addressed. e-mail: paolo.colombo@unipd.it
‡Present address: Department of Materials Science and Engineering, The Pennsylvania State University, University Park, Pennsylvania 16802.

synthesis of foams with hierarchical porosity via CAP using different catalysts (Fe, Co) and polysiloxanes.[28,31] Cellular SiOC ceramics, possessing a large amount of interconnected porosity, were produced by direct foaming, and the addition of a catalyst enabled the formation of 1D nanostructures (nanowires) in large quantity on the surface of the cell walls. In a previous work (Part I),[28] we discussed the formation of nanostructures when Fe was used as a catalyst source. It was shown that, depending on the preceramic polymer (Si:C:O ratio) and pyrolysis conditions (atmosphere and temperature), different 1D nanostructures could be obtained. In particular, when heating in N_2, single-crystal Si_3N_4 nanowires were obtained, while pyrolysis in Ar resulted in SiC nanowires. In this study (Part II), the effect of a different catalyst type (Co) is reported, and the properties of the porous components (produced with Fe or Co catalyst), including SSA values, are discussed as a function of processing conditions and catalyst type.

II. Experimental Procedure

(1) Sample Preparation

Cellular ceramics were produced by following the same procedure described in detail in Part I,[28] but using 3 wt% $CoCl_2$ (>98% pure, Sigma-Aldrich, St. Louis, MO) instead of $FeCl_2$ as a catalyst source. The precursor used was a commercially available poly(methyl-phenyl)silsesquioxane preceramic polymer (H44, Wacker Chemie AG, Burghausen, Germany). The production of porous ceramic components from the same polysiloxane precursor has already been investigated by other authors.[32] The ball-milled batch containing 1 wt% azodicarbonamide (ADA, Sigma-Aldrich) also, acting as a physical blowing agent was transferred to an oven for foaming and thermal cross linking (5 h at 250°C in air; 2°C/min heating rate). Al foil containers with variable diameters (2–4 cm) were used as a mold for the material during the cross-linking step; because a highly critical parameter is the homogeneity of the viscous blend during foaming and curing (because the addition of Co affects the cross-linking characteristics of polysiloxane precursors),[33] mixing with a thin glass spatula was performed just before the foaming, which occurred between 150° and 200°C. The porous monolithic bodies were then pyrolyzed under N_2 or Ar (both 99.999% pure) in an alumina tube furnace (2 h at the selected temperature, in the range 1250°–1400°C in 50°C steps; 2°C/min heating and cooling rate).

(2) Characterization

The true density was measured from the finely ground ceramic powder using an He-Pycnometer (Micromeritics AccuPyc 1330, Norcross, GA). Open and closed porosity of the sintered ceramics were determined by the Archimedes principle (ASTM C373-72), using xylene as a buoyant medium. Compression testing was performed at room temperature on selected pyrolyzed samples, which were cut before pyrolysis to avoid possible shape distortions. A universal testing machine (1121 UTM, Instron, Norwood, MA) using steel loading rams at a strain rate of 0.5 mm/min was used for testing. Minimum five specimens with a nominal dimension of 0.5 cm × 0.5 cm × 0.5 cm were tested per data point.

Thermal analysis measurements were carried out under Ar or N_2 (Netzsch STA 429, Selb, Germany; 2°C/min heating rate) on the already cured samples. The morphological features of the samples were analyzed from fresh fracture surfaces using a scanning electron microscope (SEM, JSM-6300F SEM, JEOL, Tokyo, Japan). SEM images were subsequently analyzed with the ImageTool software (UTHSCSA, University of Texas, TX, USA) to quantify the cell size, cell size distribution, nanowire length, and diameter. The raw data obtained by image analysis were converted to 3D values to obtain the effective cell dimension by applying the stereological equation: $D_{sphere} = D_{circle}/0.785$.[34] Specimens appropriate for high-resolution transmission electron microscopy (HRTEM) were prepared using an adapted cross-sectioning technique. Atomically resolved characterization as well as electron energy loss (EELS) and energy-dispersive X-ray spectroscopy (EDXS) was performed using an aberration-corrected (C_s probe corrector) FEI TITAN 80-300 analytical scanning transmission electron microscope (FEI, Hillsboro, OR), allowing a spatial resolution of better than 1 Å in STEM mode and an energy resolution of the EELS measurements of about 0.2 eV, which was of special importance for the recording of the fine-structure signals near the ionization edges, yielding information on chemical bonding. The microstructures of some selected samples were investigated using a Philips CM 20 field-emission gun (FEG, Philips Electron Optics, Eindhoven, the Netherlands) microscope, operating at 200 keV with a point-to-point resolution of 0.24 nm and equipped with both a Gatan Imaging Filter (GIF 200, Model 667, Gatan Inc., Warrendale, PA) and an EDX detector enabling the detection of light elements (IDFix-system, SAMx, Bruchsal, Germany). X-ray diffraction data (XRD, Bruker D8-Advance, Karlsruhe, Germany) were collected using Cu$K\alpha$1 radiation (40 kV, 40 mA, step scan of 0.05°, counting time of 5 s/step). Raman spectra were recorded with an Invia Raman microspectrometer (Renishaw plc., Gloucesteshire, U.K.) attached to a confocal microscope (× 50 objective) using the 633 nm line of an He–Ne laser as the excitation wavelength. Samples were ground and the powders were used for analysis, using a low laser power (5%).

Nitrogen adsorption/desorption at 77 K was measured using a Micromeritics ASAP 2020 system (Micromeritics Inc., Norcross, GA). The sample was first degassed under high vacuum (3×10^{-3} mbar) at 400°C for 15 h and then was transferred to the analysis system for the free-space measurement with helium. Thereafter, the sample was again degassed under vacuum at 400°C for further 2 h, before sorption analysis. SSA was calculated from N_2 adsorption data at relative pressures below 0.20, by the multipoint Brunauer–Emmett–Teller (BET) method. Data were also analyzed by the *t*-plot method and by the Barrett–Joyner–Halenda (BJH) method, using the manufacturer's software. The apparent micropore distribution was calculated from N_2 adsorption data by the Horvath–Kawazoe method.

III. Results and Discussion

(1) Thermal Analysis

The curing process yielded thermoset foam with high porosity, which could be pyrolyzed to high temperature without important change in morphology or formation of cracks. Thermogravimetric analysis (see Figs. 1(a) and (b)) showed that samples containing Co ions had a higher weight loss than those with Fe ions (e.g., ~30 and ~22 wt%, respectively, at 1200°C in N_2), and that the weight loss depended on the heating atmosphere (weight loss was higher when heating in Ar). The sample containing $CoCl_2$, analyzed in N_2, also showed an endothermic decomposition peak at a temperature ~1450°C, similar to what

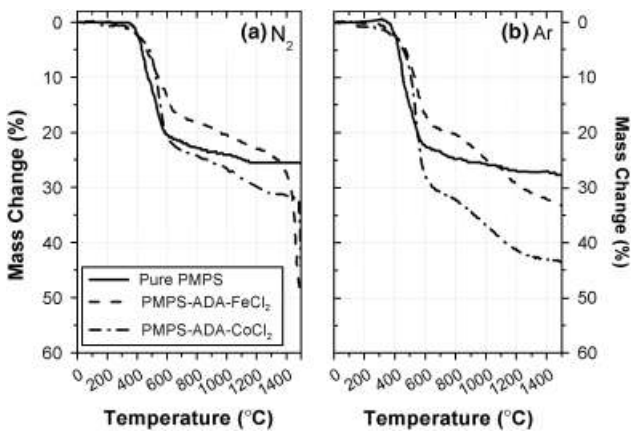

Fig. 1. Thermogravimetric analysis data for poly(methyl-phenyl) silsesquioxane samples treated under (a) N_2 and (b) Ar.

was observed for the sample catalyzed with Fe ions. This enhanced decomposition (decrease in thermal stability) resulted in the release of gaseous byproducts (SiO and CO), similar to what was reported for a or Ni-containing polysiloxane.[22] A more detailed investigation of the effect of different metal ions on the weight loss of the polysiloxane precursor was, however, outside the scope of the present study.[33,35]

(2) Morphology

The general morphology of the ceramic samples produced using $CoCl_2$ as a catalyst was very similar to that of samples containing $FeCl_2$, indicating that these metal ions had a similar effect, if any, on the decomposition of the physical blowing agent and the low-temperature rheology of the polysiloxane precursor. As expected, no significant change could be observed in the morphology at the macroscale for samples heated between 1250° and 1400°C. The total porosity of the samples was always higher than 70 vol% (open porosity was always at least 80% of the total porosity), and preliminary compression tests showed that the pyrolyzed foams had a compression strength below 2 MPa. For the samples pyrolyzed at low temperature (1250°C), SEM investigations showed the presence of only a low amount of 1D nanostructures scattered on the cell walls, most probably because of the limited amount of gases generated at this pyrolysis temperature. Above this temperature, the microstructure of the pyrolyzed samples started differing at the microscopic level, depending on the heating atmosphere and temperature. All the samples contained a large amount of nanowires (see images in Figs. 2(a)–(f) and 3(a)–(f)) protruding from the cell walls. SEM investigations revealed that the nanowire length was affected by the pyrolysis temperature (as high as 300 μm nanowires were obtained by 1400°C/N_2 pyrolysis). A decrease in the cell size and cell window diameter with the increasing pyrolysis temperature was observed under both pyrolysis atmospheres, due to the shrinkage, which preceramic polymer systems undergo during heating, and at 1400°C under N_2 foams having spherical cells (483.4 ± 225.6 μm in diameter) with connecting cell windows (128.6 ± 105.6 μm in diameter) were obtained. These results are comparable with those for the samples produced by using Fe as a catalyst source. After pyrolysis at 1300°C under N_2, nanowire bundles homogeneously distributed on the cell walls could be observed (see Figs. 2(a) and (b)). Bundle-like formation of nanowires (Si_3N_4, see later) has already been observed by other researchers,[36,37] and it has recently been proposed that the controlling parameter for the development of this nanostructural morphology is dictated by the growth mechanism, i.e. VLS (see later).[36] As the nanowires originate from Co particles, at 1300°C, they are concentrated only on specific locations on the cell walls. Increasing the temperature caused an increase in the dimension and number of these bundles, resulting in a full coverage of the cell wall surfaces at 1350°C (Figs. 2(c) and (d)), followed by the formation of long, straight nanowires connecting the different bundles (see Figs. 2(e) and (f)). The diameter of the nanowires was computed by image analysis from an average of 200 measurements per each sample. Upon pyrolysis at 1400°C under N_2, nanowires with an average diameter of 100.13 ± 33.38 nm were produced.

The samples pyrolyzed under Ar had the cell walls uniformly coated with nanowires too (see Figs. 3(a)–(f) for SEM micrographs of samples pyrolyzed at 1300°, 1350°, and 1400°C, respectively), but their morphology and composition were different from those produced when heating in N_2. In fact, these nanofibers appeared to be 128.68 ± 33.06 nm in diameter and generally < 50 μm in length (shorter than those produced when heating in N_2) and were not amassed in bundles but formed some small entanglements (see Figs. 3(e) and (f)), differently to what observed for Fe-containing samples.[28]

(3) Structural Characterization

The XRD and Raman patterns of the samples pyrolyzed at different temperature in N_2 are reported in Fig. 4 (left) and (right), respectively. The samples pyrolyzed at 1250°–1300°C showed the presence of a broad hump in the 20°–30° (2θ) region, which could be assigned to the amorphous silicate phase,[38] clearly defined crystalline peaks attributable to β-SiC (JCPDS #29-1129), cobalt silicide CoSi (JCPDS #72-1328), and a broad peak at 2θ ~26° (corresponding to the (002) plane of graphite) implying the precipitation of graphite-like carbon (labeled as "C" in graph). At this temperature, peaks attributable to the Si_3N_4 phase are also present, and they are linked to the formation of nanowires. It is known that above 1200°C, the SiOC glass network undergoes a phase separation process with a reduction of mixed SiOC units, an increase of the [SiC_4] and [SiO_4] units, and the ordering of the free carbon phase.[38–40] Consequently, we can attribute the observation of these primary phases (SiC and graphite-like carbon) in the samples treated at low temperature (1250°C) to the phase separation process. The broad peak corresponding to the carbon phase decreased in intensity with the increasing thermolysis temperature, concurrently with the increase in the peak intensity of the SiC phase.

Raman spectroscopy was used to acquire information about the structural evolution of the free carbon phase dispersed in the

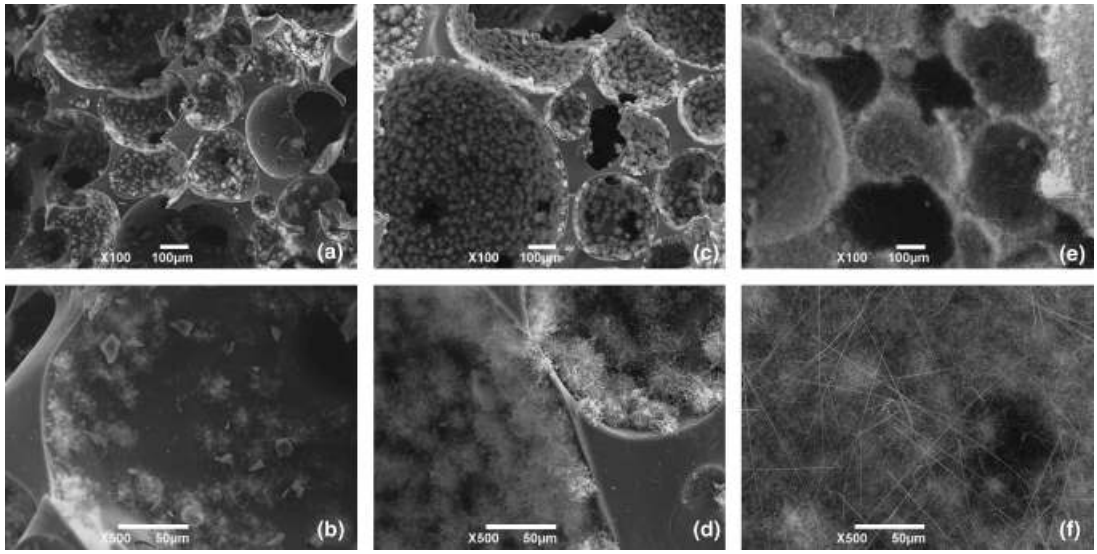

Fig. 2. Scanning electron micrographs taken from the fracture surfaces of sample poly(methyl-phenyl)silsesquioxane–$CoCl_2$–azodicarbonamide pyrolyzed under N_2: (a and b) at 1300°C, (c and d) 1350°C, and (e and f) 1400°C.

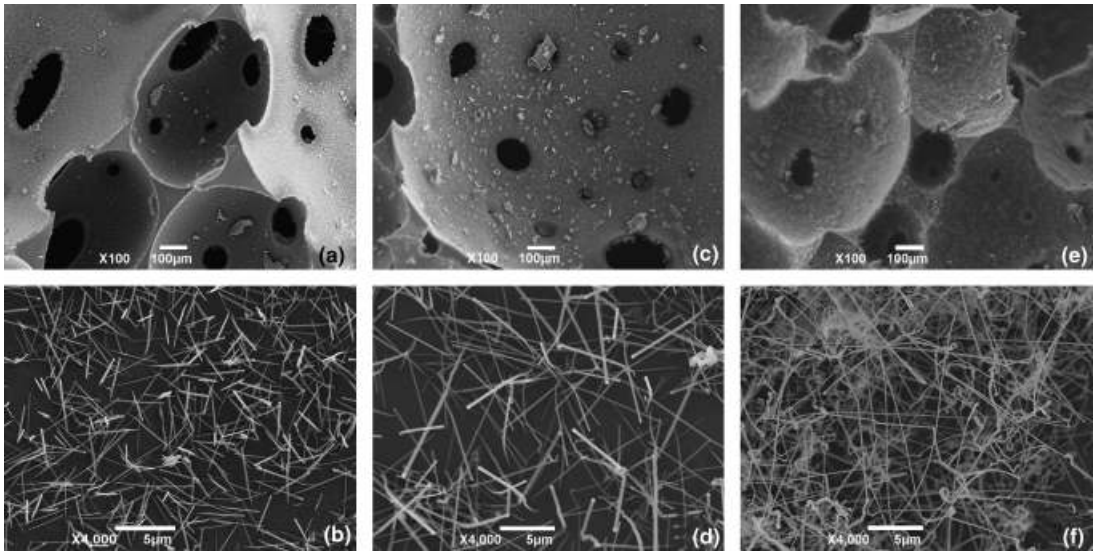

Fig. 3. Scanning electron micrographs taken from the fracture surfaces of sample poly(methyl-phenyl)silsesquioxane–$CoCl_2$–azodicarbonamide pyrolyzed under Ar: (a and b) at 1300°C, (c and d) 1350°C, and (e and f) 1400°C.

matrix, at different pyrolysis temperatures. Data show that, at low temperature (1250°C), the sample had the characteristic bands observed in disordered sp^2 carbon, D ($\sim$1330 cm^{-1}, breathing mode) and "graphite-like" G near $\sim$1590 cm^{-1} (in plane vibrational mode). In this spectrum, the distinct shoulder at $\sim$1620 cm^{-1}, close to the G band, is attributed to the D′ band, which is generally ascribed to defected or nanocrystalline graphite in PDC materials.[41,42] It is known that the position of the G band gives information on the type of disordered carbon (amorphous versus nanocrystalline) present. Values close to 1600 cm^{-1} suggest the presence of a nanocrystalline form of graphite, rather than amorphous carbon.[41,43] Thus, the observed characteristics of the Raman spectra indicate that nanocrystalline graphite-like carbon was already present in the sample pyrolyzed at 1250°C, as supported also by XRD observations. Heat treatment at higher temperatures did not affect the arrangement of the free carbon phase significantly. The corresponding spectrums are also characterized by similar peaks in almost the same positions, with a slight increase in I(D)/I(G) ratio which went from 1.63 (1250°C) to 1.72 (1400°C), suggesting a decrease in the in-plane cluster size (La) of carbon regions.[44] The data demonstrate the permanence of carbon in the samples at all pyrolysis temperatures, as already observed for Fe-containing samples[28] and are further corroborated by HRTEM (see later).

Pyrolysis at 1400°C resulted in a ceramic-containing β-SiC, Si_3N_4 (both α (JCPDS #41-0360), and β (JCPDS #33-1160) polymorphs), CoSi, and a disordered carbon phase. The peak located at 33.7° could be assigned both to the stacking faults in the β-SiC crystalline structure[45] and to the (101) plane of β-Si_3N_4. No oxynitride phase was observed, and clearly carbon and amorphous silica (or SiOC) were consumed with the increase in the pyrolysis temperature. Supporting the findings of Siddiqi and Hendry,[46] it was observed by Yu *et al.*[47] that the crystallization of preceramic polymer-derived amorphous Si_2N_2O residue results in different products, namely either Si_2N_2O or α-Si_3N_4–Si_2N_2O mixture depending on the C:O ratio. While a high C:O ratio involves the consumption of oxygen during crystallization, and therefore Si_3N_4 is produced, a low C:O ratio enables the formation of Si_2N_2O. Indeed, parallel experiments performed using a low carbon-containing polysiloxane (MK, Wacker Chemie AG, Munich, Germany, carbon $\sim$13 wt%[48]) and a similar catalyst source yielded Si_2N_2O.[31] This implies that in the present experimental conditions (i.e., the use of a high carbon-containing precursor, H44, carbon $\sim$40 wt%[48]), the partial pressure of oxygen was always kept lower than that required to form Si_2N_2O.

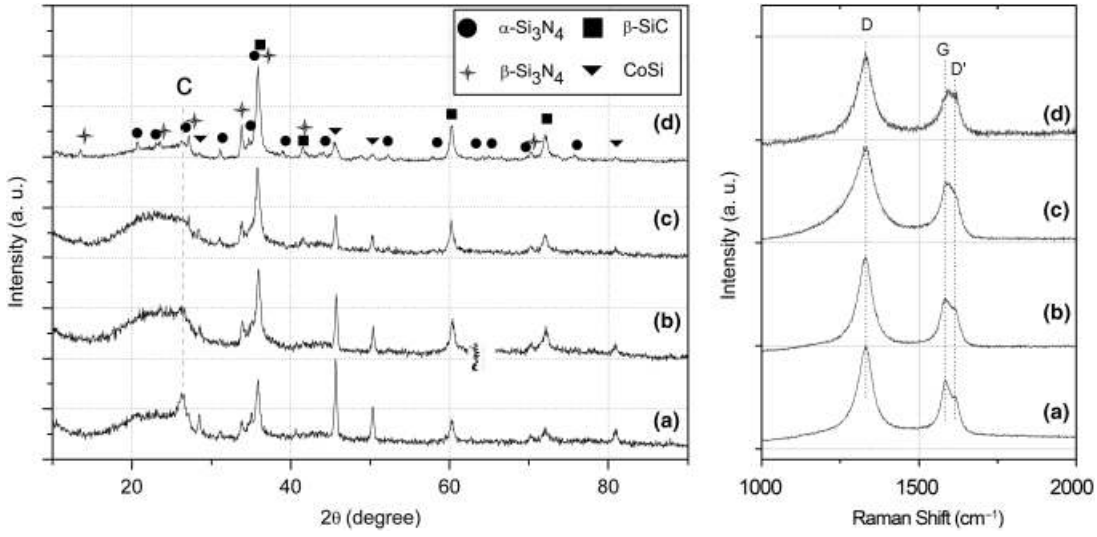

Fig. 4. X-ray diffraction patterns (left) and Raman spectroscopy (right) of the samples pyrolyzed in N_2 (a) at 1250°C, (b) 1300°C, (c) 1350°C, and (d) 1400°C treatment.

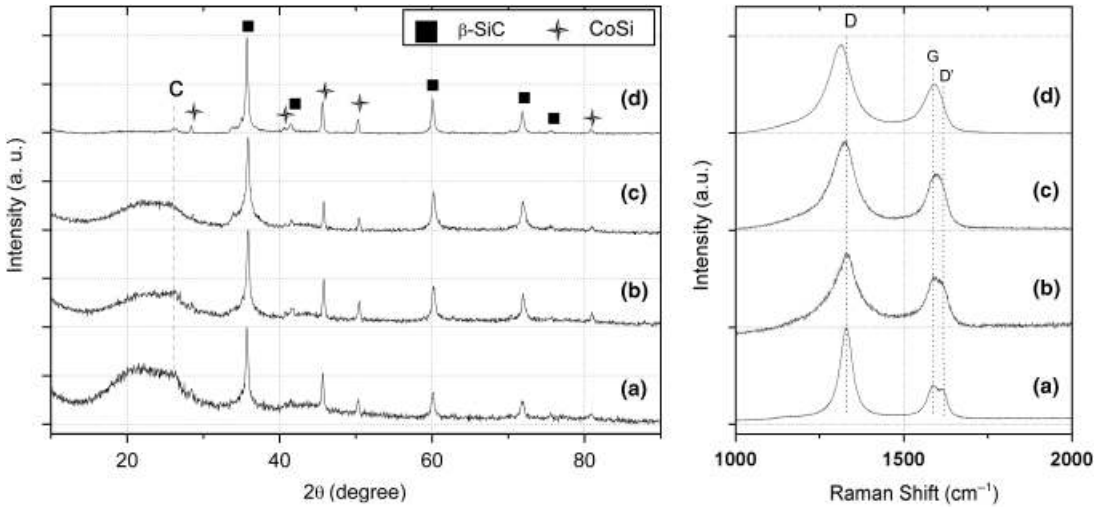

Fig. 5. X-ray diffraction patterns (left) and Raman spectroscopy (right) of the samples pyrolyzed in Ar (a) at 1250°C, (b) 1300°C, (c) 1350°C, and (d) 1400°C treatment.

Figure 5 (left) and (right) reports the XRD and Raman patterns of samples heated at different temperatures in Ar, respectively. Samples pyrolyzed at 1250°–1350°C showed again the presence of a broad hump in the 20°–30° (2θ, amorphous silicate phase), β-SiC and CoSi peaks, while the broad peak related to carbon (~26°) was less evident. As observed for all other samples, an increase in pyrolysis temperature promoted better SiC crystallization. The depression of the hump corresponding to the silicate phase suggests similarly that SiC formed at the expense of amorphous silica via a carbothermal reduction mechanism. Raman data, at low temperature (1250°C), show narrow D (~1330 cm^{-1}), G (~1590 cm^{-1}), and D′ (1620 cm^{-1}) peaks, implying the precipitation of highly defective graphite-like carbon.[41] The corresponding spectrum at 1300°C is also characterized by similar peaks in almost the same positions, with a broadening in D peak (FMHW from 44 to 110 cm^{-1}). Starting from this temperature, with the increasing pyrolysis temperature, the I(D)/I(G) ratio increased from 1.56 (1300°C) to 1.79 (1400°C) and the D peak slightly shifted to lower frequencies (see Fig. 5 (right, d)). This suggests a decrease in size and a probable increase in disordering of existing nanocrystallites. The permanence of disordered carbon phase was confirmed by Raman spectroscopy in the samples at all pyrolysis temperatures, similarly to the treatment in N_2, as already observed for Fe-containing samples[28] and further corroborated by HRTEM. Pyrolysis at 1400°C in Ar atmosphere, therefore, resulted in a multiphase SiOC ceramic-containing β-SiC and CoSi crystals, together with a free carbon phase.

CoSi formed at all pyrolysis temperatures in both Ar and N_2 atmospheres, similar to what was observed for the samples containing iron, in which iron silicide phases were obtained, because of the good affinity between the two elements, as found also when joining Si-containing ceramics to cobalt or its alloys by solid-state bonding.[49] The reduction of $CoCl_2$ to micrometer-sized metallic Co particles during heating in inert atmosphere and their interaction with the silicon-containing matrix were responsible for the formation of CoSi.[35,50] XRD analysis performed on samples prepared at lower temperatures (500°–1200°C in 100°C steps, data not shown) demonstrated that CoSi started to form above around 1200°C, parallel to the findings of Bourg *et al.*[35]

(4) Nanochemical Characterization

HRTEM investigations combined with EDX measurements enabled to determine the nanochemical composition of the nanowires and to ascertain their growth mechanism. An HRTEM image of an Si_3N_4 nanowire formed on a cell wall of a sample pyrolyzed at 1400°C in N_2 is reported in Fig. 6(a). The EDX profile taken from the body of the nanowire (Fig. 4, bottom left) indicated that the nanowire contained only Si and N elements. The caps of the nanowires consisted of cobalt silicide of varying stoichiometry (around 1:1), as revealed by their typical EDX spectrum (Fig. 6, bottom right), in good agreement with the XRD result. A higher magnification HRTEM image, reported in Fig. 6(b), shows that the nanowire had a perfect single-crystal α-Si_3N_4 structure, without defects (as confirmed also by the selected-area electron diffraction pattern (SAED)—see inset), which was identical over the entire wire length. This observation is consistent with the recent results obtained from polysilazane samples containing Fe.[36,51] The HRTEM image together with the SAED pattern suggest that the nanowire grew along the [1–10] direction (see arrow). The factors controlling the transformation between Si_3N_4 polymorphs (α to β) are very complex,[52,53] especially for complex multiphase systems like those of the present study. We can briefly comment, however, that generally this transformation occurs at temperatures ≥1300°C, unless the local SiO partial pressure within the reacting material is high, in which case the α polymorph is stable over the β one up to the nitride decomposition temperature, leading to the formation of SiC.[52] Therefore, we posit that the β polymorph (high-temperature polymorph) observed by XRD formed in some local areas in which the SiO partial pressure was not high enough to stabilize α-Si_3N_4. Although the transformation from Si_2N_2O phase to Si_3N_4 is a common phenomenon,[52] we can exclude that this occurred in the present system, because XRD data for samples pyrolyzed at lower temperatures (800°–1200°C in 100°C steps) did not show the presence of Si_2ON_2, unless of course such phase was amorphous.

Because the melting point of nanoclusters is lower than that of the corresponding bulk solids,[54] it is plausible to assume that in these experiments CoSi (T_m = 1480°C) was in a pseudoliquid state above 1250°C (note that nanowires were obtained only when heating at temperatures ≥1250°C, which is also high enough to cause SiO volatilization from the SiOC matrix[40,55]). It is known that the surface of these liquid droplets has a large accommodation coefficient, and therefore they are a preferred deposition site for the incoming SiO and CO gases,[24] which form during pyrolysis of the polysiloxane preceramic polymer,[35,40,55] and for nitrogen from the heating atmosphere. The incorporation of these gases may lead to a supersaturation of the liquid phase in the elements forming the crystals (SiC, Si_3N_4).[56–59] The presence of catalyst droplets at the tips of the Si_3N_4 nanowires (Fig. 4(a)), together with the fact that nanowires were obtained only when Co was present, indicates that the growth proceeded through a solution precipitation (VLS) mechanism.[36,59,60] The

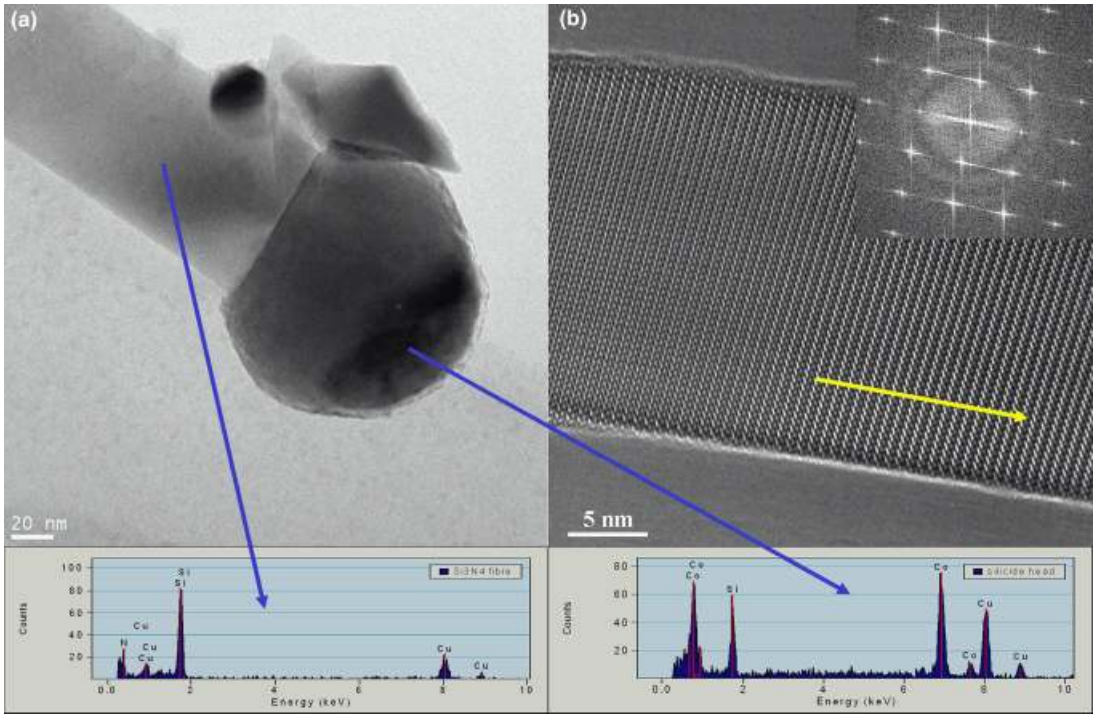

Fig. 6. High-resolution transmission electron microscopy (HRTEM)/energy dispersive X-ray (EDX) spectroscopic analyses of a sample pyrolyzed at 1400°C under N_2; (a) overview with corresponding nanochemical data: EDX (bottom left) of nanowire, and EDX (bottom right) of nanowire tip (Cu comes from TEM grid), (b) HRTEM image showing the regularity at the atomic scale of the nanowire body, with diffraction pattern (inset).

growth mechanism for the Si_3N_4 nanowires, therefore, differed from what was observed when $FeCl_2$ was used as a catalyst source under the same experimental conditions. This is most probably due to the different silicide phase, i.e. different content of silicon in the silicide phase. Generally, similar results, but different conclusions, have been reported for catalyst systems in which Ni, Co, and Fe react on Si substrates forming metal silicides.[61] Various parameters can affect the catalytic activity; for example, Esconjauregui *et al.*[61] have very recently shown the importance of particle topography on the catalytic activity of metal silicides (silicon-rich Ni or Co silicides) to produce CNTs. Yang *et al.*[56] reported that while metal-rich silicides (such as Fe_3Si) are not suitable for the precipitation of SiC, silicon-rich melts (such as CoSi) can be successfully used to produce SiC crystals. In this manner, Li *et al.*[57] obtained α-Si_3N_4 nanowires from high-energy ball-milled Si powder via thermolysis under N_2. The produced nanowires had silicon-rich ($FeSi_2$) metallic tips, and the common VLS mechanism was proposed for their formation. Together with previously published results on the catalytic activity of different metal silicide phases, our results illustrate that the stoichiometry of the metal (Fe or Co) silicide compound (i.e., metal-rich or silicon-rich) is a key controlling parameter for the precipitation of SiC and Si_3N_4 crystals via VLS.[28,56,57] In fact, when Fe-containing samples were treated under N_2, the formed silicide phase was always rich in metal (predominantly Fe_3Si), and precipitation from this phase was hindered due to the inability of carrying the liquid to saturation with respect to Si, C, and N.[28,56] On the other side, the use of Co catalyst resulted in an Si-rich (CoSi) silicide phase, which acts as a suitable medium for the saturation with Si, C, and N. In the next stage, then Si_3N_4 nanowires precipitated from this supersaturated liquid droplet. The reason why only Si_3N_4 (and not SiC) nanowires formed is simply because Si_3N_4 is thermodynamically more stable over SiC up to ~1450°C in the presence of 0.1 MPa N_2 (i.e., the present experimental conditions).[62,63]

Similar investigations also enabled to ascertain the nanochemical composition of the nanowires and their growth mechanism when the sample was pyrolyzed in Ar at 1400°C (see Figs. 7(a) and (b)). The caps of the nanowires consisted again of cobalt silicide of varying stoichiometry (around 1:1 as revealed by their EDX spectrum, data not shown) in agreement with the XRD data. The nanowires contained only Si and C (see EDX spectra in Fig. 7(a), bottom left) and the electron diffraction pattern (Fig. 7(b), top right) together with the XRD data revealed that they were comprised of β-SiC. The arrangement of the atomic planes of the SiC nanowires observed by HRTEM (Fig. 7(b), top right) indicated that the growth direction of the nanowire is orthogonal to the {111} planes of SiC (the arrow in Fig. 7(b) shows the growth direction of the nanowire). This observed growth direction is indeed typical of SiC nanowires grown by a solution–precipitation mechanism.[24,62,64] In some cases, the SiC nanowires contained arrays of planar defects, also resulting in characteristic multiple reflexes in the diffraction pattern (see SAED pattern in Fig. 7(b), top right), as highlighted by the XRD results and previous investigations.[24,28,65]

It has been shown that the formation of a Co–Si liquid phase is essential for the nucleation and growth of SiC, because of a high carbon solubility in it at high temperatures.[66,67] As in the case for N_2 pyrolysis, due to quantum effect for the nanoparticle catalysts,[24,54] pseudoliquid CoSi droplets formed during pyrolysis. The formation of a supersaturated solution with respect to Si and C atoms then occurred, from which solid-phase SiC crystals nucleated via precipitation, followed by growth along the more thermodynamically favorable direction (i.e., ⟨111⟩). Therefore, combining XRD, SEM (coupled with EDS analysis (data not shown)), and HRTEM (coupled with EDX analysis), we can conclude that the SiC nanofibers grew via the well-known VLS mechanism,[60] with Co acting as the metal catalyst similar to what was found for the Fe-containing samples pyrolyzed under Ar.[28] Narciso-Romero and Rodríguez-Reinoso[67] compared the synthesis of SiC whiskers from rice hulks using different catalyst sources (Fe, Co, and Ni), and showed an increasing order of catalytic activity, in terms of reaction rate, according to Ni > Co > Fe. Comparing the images of the fracture surfaces of samples produced using the two different catalysts (assuming that the distribution of nanowires were homogenous on both surfaces upon fracture), we can confirm that the catalytic effect of Co was higher than that of Fe, leading to the formation of a larger amount of SiC nanowires during pyrolysis under Ar atmosphere.

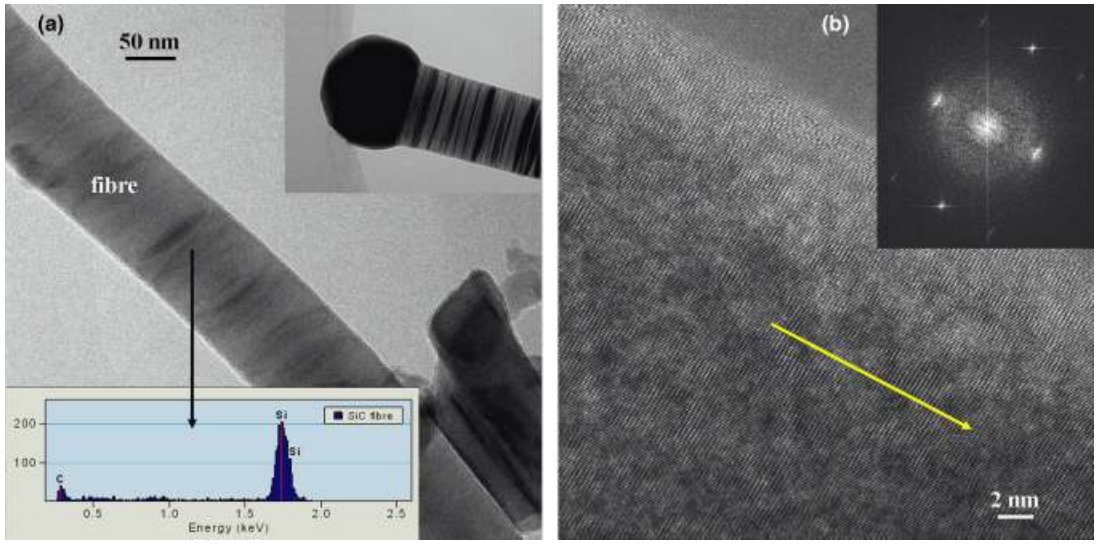

Fig. 7. High-resolution transmission electron microscopy/energy dispersive X-ray (EDX) spectroscopic analyses of a sample pyrolyzed at 1400°C under Ar; (a) fiber overview and related EDX spectra (bottom left) taken from body of the nanowire. Top right inset shows the smooth interface between metallic cap and nanowire; (b) magnification showing the growth direction (arrow) orthogonal to {111} SiC planes; inset reports the selected-area electron diffraction pattern showing characteristic multiple reflexes caused by planar defects in the nanowire due to SiC polytypism.

FEG–TEM analyses were also performed on the cell wall surfaces, in order to investigate their nanochemical and microstructural features. In Fig. 8 is reported a FEG–TEM image taken from the cell wall surface of a sample heated at 1400°C in N_2, in the vicinity of a nanowire. It reveals that the amorphous matrix phase contained nanocrystalline SiC, and a few areas of nanocrystalline graphite-like carbon (as indicated also by Raman investigations), while no micro- (< 2 nm) and meso- (between 2 and 50 nm) pores were found. The EDX spectrum (right) shows that the matrix phase consisted only of silicon, carbon, and oxygen atoms thereby confirming, together with previous HRTEM analyses, that nitrogen was always present in the nanowires. Also, no Co was found in the ceramic foam, but always only at the tip of the nanowires.

Similarly, no porosity was found in the ceramic cell wall of a sample heated at 1400°C in Ar (see Fig. 9). Compared with pyrolysis in N_2, larger (10–20 nm) and more frequent crystalline SiC regions together with nanocrystalline graphite-like carbon areas could be observed. As expected, EDX analysis gave only silicon, carbon, and oxygen.

(5) Porosity and SSA

As detailed in the experimental section, in order to perform accurate physisorption measurements, a second outgassing step was conducted after the determination of the free space with helium. This procedure is usually adopted in the case of materials containing micropores to assure that the sample adsorption sites are completely free from entrapped helium. In a standard procedure for mesoporous materials (2 nm < pore size < 50 nm) analysis, the adsorption of helium is considered negligible. But in the case of the samples produced in the present study, the presence of micropores (pore size < 2 nm) could be envisaged, as a result of nanowire growth and assemblage. Taking also into consideration that no micro/mesoporosity was found by FEG–TEM in the cell walls of the ceramic foams heated in both atmospheres (see Figs. 8 and 9), we can consider that in our samples the "pores" are constituted simply by the interspaces among the nanowires and between the nanowires and the cell walls.[5,7,10] Therefore, data concerning pore size and volume, obtained from BET analysis, are not linked to the actual presence of physical pores in the ceramic skeleton, and the pore shape approximation can result only in a rough estimate of these values. The nitrogen adsorption–desorption isotherms (77 K) of samples containing Co or Fe, heated under Ar or N_2 at 1400°C, are reported in Figs. 10(a) and (b). The samples containing Fe as a catalyst were produced in previous experiments.[28] For the sake of comparison, the isotherm for the pure matrix H44 (1400°C, Ar) was also included in the plot. The curves for the pure samples without metallic catalytic particles pyrolyzed at 1400°C exhibited an isotherm close to Type II (IUPAC classification), with no hysteresis loop and almost negligible N_2 adsorption up to very high

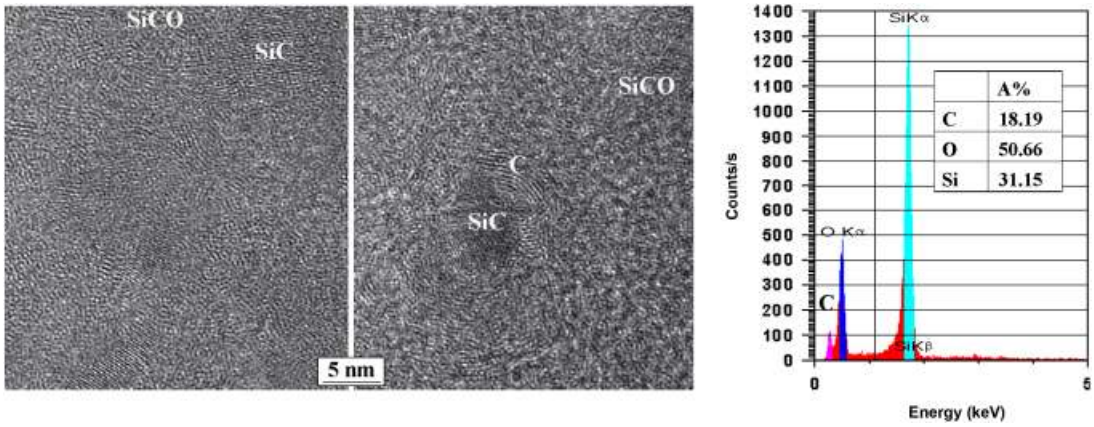

Fig. 8. Field emission gun–transmission electron microscopic image taken from the cell wall surface of a sample pyrolyzed at 1400°C under N_2 (left), and energy dispersive X-ray spectrum (recorded from the whole area at an average, right).

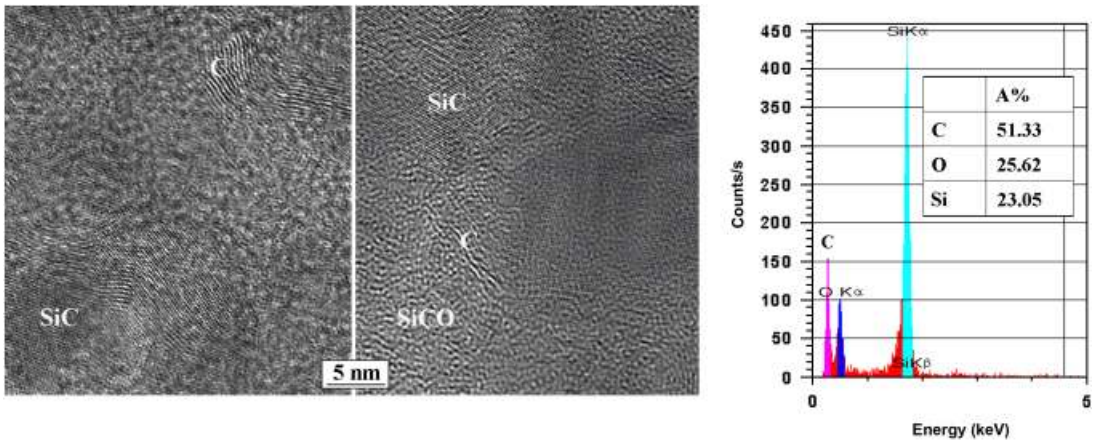

Fig. 9. Field emission gun–transmission electron microscopic image taken from the cell wall surface of a sample pyrolyzed at 1400°C under Ar (left), and energy dispersive X-ray spectrum (recorded from the whole area at an average, right).

relative pressure, where a slight N_2 uptake is visible, owing to multilayer adsorption on macropores. The curves for samples including catalytic metal ions indicated a different behavior. Interestingly, the isotherms for Co including samples are close in shape to Type IV, with hysteresis loops that can be assigned to type H1 in the case of samples heated in Ar, and H3 in the case of samples heated in N_2. Type H1 loops are often an indication of both high pore size uniformity and high pore connectivity. In this case, the mesopores result from interstices between close packed, regularly arranged ceramic nanowires, and from the spaces between the nanowires and the cell walls. In the case of Co samples treated in N_2, nanowire bundles were produced together with longer and straight single nanowires, as shown in the SEM images (see Figs. 2(e) and (f)), which protrude from the cell walls for hundreds of micrometers and arrange on the cell surface in a highly disordered fashion. This is reflected by the isotherm shape, where the hysteresis loop starts at lower relative pressures ($p/p_0 \approx 0.43$) and does not close until the saturation vapor pressure is reached. It is well known that type H3 loops have been generally obtained with plate-like particles or slit-shaped pores.[68,69] Here, we can consider the spaces between the nanowires as wedge- and slit-shaped pores, where the high packing density hampers the mesochannels connectivity. The size distribution of the mesopores of Co samples heated in Ar or N_2 at 1400°C was obtained through the BJH method, and are reported in the inset of Fig. 10(a). As it can be observed, pyrolysis in N_2 gave narrower mesopores with respect to Ar treatment (7.8 vs 15.0 nm, as determined from the BJH model applied to the desorption branch), thus confirming a tighter packing of the nanowires. In both cases, N_2 or Ar treatment, the isotherms of samples containing Co displayed a moderate N_2 uptake in the low pressure range, as highlighted in Fig. 10(b), associated with the presence of microporosity. The application of the *t*-plot method, using a thickness curve-type Harkins and Jura allowed to confirm that a significant fraction of micropores was present in the multiphase SiOC ceramic composites. The micropore volume increased steadily with the treatment temperature up to 1350°C, whereas the micropores size, as derived from HK model, kept almost constant at 0.7 nm. Hence, it can be concluded that the Co samples possessed hierarchically porous (trimodal) architecture, with the coexistence of micro-, meso-, and macropores. The N_2 adsorption–desorption curves for samples containing Fe exhibited mainly a Type II behavior, with gradual N_2 uptake at moderate pressure (p/p_0) and a predominant N_2 adsorption at high p/p_0, associated with the presence of macropores. The hysteresis loop (type H3) is very narrow, the adsorption and desorption branches being almost vertical and nearly parallel above 0.8 of the relative pressure, confirming the presence of a significant external surface. In both pyrolysis atmospheres, Fe-containing samples heated at 1400°C presented broad pore size distributions, peaking at 11.6 nm for the N_2-treated sample and 22.6 nm for the Ar-treated sample, as derived via the BJH model applied to the desorption branches of the isotherms. This is in good agreement with the large variability in the shape and volume of the voids among the nanowires themselves.

The SSA value for the foam substrate (containing no catalyst and in the expanded—with ADA—and nonexpanded form),

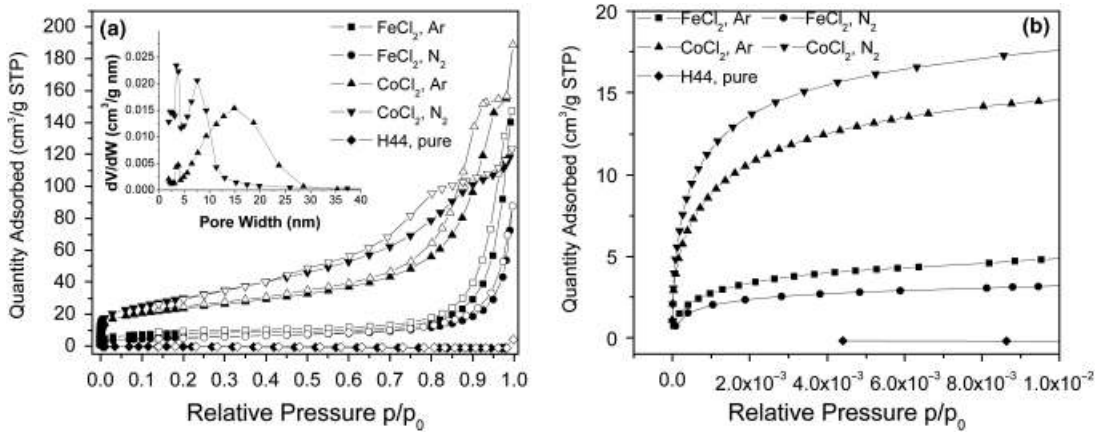

Fig. 10. Nitrogen adsorption isotherms (77 K) of samples containing Co or Fe, heated under Ar or N_2 at 1400°C. For the sake of comparison, the isotherm for the pure matrix H44 (1400°C, Ar) is included in the graph. The solid and open symbols indicate adsorption and desorption branches, respectively. (a) Full isotherm and pore size distribution of Co samples (inset); (b) expanded view of low-pressure region.

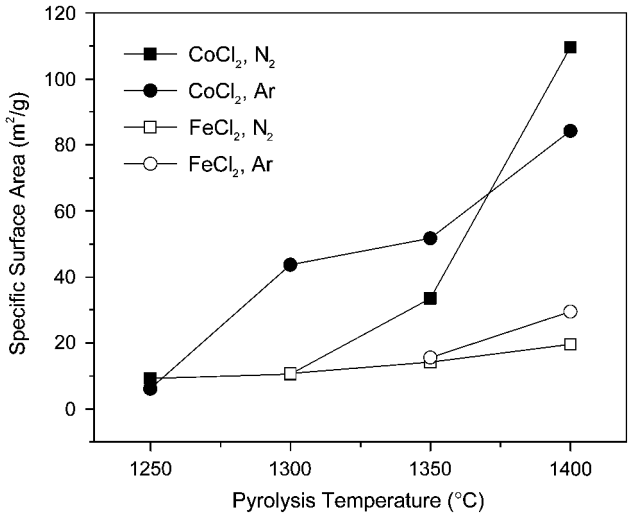

Fig. 11. Plot of specific surface area (from Bruna1uer–Emmett–Teller regression analysis) vs. pyrolysis temperature for samples H44-$CoCl_2$ and H44-$FeCl_2$, heated either in N_2 or Ar at 1400°C.

heated in Ar at 1400°C, was <1 m^2/g. As a general trend, the samples containing Co gave higher SSA values in comparison with those containing Fe (see Fig. 11). Moreover, while the samples heated below 1300°C had always low SSA values ($< \sim 10$ m^2/g), the ones produced at higher temperatures resulted in a high SSA samples (10–110 m^2/g). The highest value of SSA, 109.5 m^2/g, was obtained for a sample containing Co and pyrolyzed at 1400°C under N_2.

Our results are in accordance with the literature. Jarrah *et al.*[6,7] deposited CNFs on the cell walls of γ-alumina washcoated cordierite honeycombs, and showed that the SSA could be increased from 45 to 63 m^2/g, because of the presence of a ~1-μm-thick layer of CNFs (diameter of 10–30 nm). The fiber diameter was controlled by the size of the deposited Ni particle, the reactivity of the gas in contact with the particle, and the duration of thermal treatment, and this parameter, together with the total amount of fibers formed, affected the final SSA of the component.[7] BET analysis showed the presence of micropores, which were attributed by the authors to the space between the fibers and the pore walls of the washcoat layer, which contained only mesopores (5–20 nm).[7] de Lathouder *et al.*[9,10] followed a similar strategy and demonstrated that CNF-containing cordierite monoliths possessed ~8 nm mesopores, which were again attributed to the space among the fibers and therefore not to the presence of pores in the substrate. It was also shown that a correlation between fiber diameter and the SSA values existed (assuming a constant carbon yield), according to which an increase in the fiber diameter caused a decrease in the surface area.[10] Other researchers also underlined the significant influence of the diameter and degree of entanglement of the CNFs on the resulting SSA of the macroporous ceramics on which they were deposited.[8] Vanhaecke *et al.*[4] showed that the conversion of such a CNF layer into SiC (via reaction with gaseous SiO) resulted in a decrease of the SSA value, because of the increase of the nanofibers diameter after reaction.

We can therefore attribute the observed differences in the SSA values with the heating temperature, the type of catalyst, and the type of pyrolysis atmosphere to the variation in the amount and morphology (diameter, length, and degree of entanglement) of the formed nanowires. In fact, Co catalyst produced thinner nanowires (100.13 ± 33.38 nm in N_2; 128.68 ± 33.06 nm in Ar; samples heated at 1400°C) than those obtained from Fe (154.47 ± 43.04 nm in N_2; 280.23 ± 120.3 nm in Ar; samples heated at 1400°C). This confirms that SSA increases with the decreasing diameter of the nanofibers. Moreover, the pyrolysis in N_2 of Co-containing samples formed bundles of Si_3N_4 nanowires (see Figs. 2(a)–(f)). This particular morphology was caused most probably by multiple nucleation on a same large Co particle, as observed for Si_3N_4 nanowire bundles produced using Fe particles in the pyrolysis polysilazane precursor,[36] while straight nanowires formed starting from smaller droplets (see Figs. 2(e) and (f)).

In conclusion, the high SSA values observed in our samples derive from the presence of additional surface provided by the nanowires. A schematic mechanism for the formation of the nanowires, with the concurrent development of micro- and meso-"pores" (i.e., the space among the nanowires and between nanowires and solid foam skeleton), is shown in Fig. 12. We envision that the ceramic components with hierarchical porosity that we produced in this work could be used for several applications, including trapping of (nano)particles, gas adsorption, or catalysis (e.g., Fischer Tropsch synthesis or N_2O decomposition).

IV. Conclusions

The pyrolysis of a foamed silicone resin containing 3 wt% $CoCl_2$, resulted in highly porous (>70 vol%) SiOC ceramics possessing dense cell walls decorated with nanowires. The composition and morphology of the nanowires depended on the

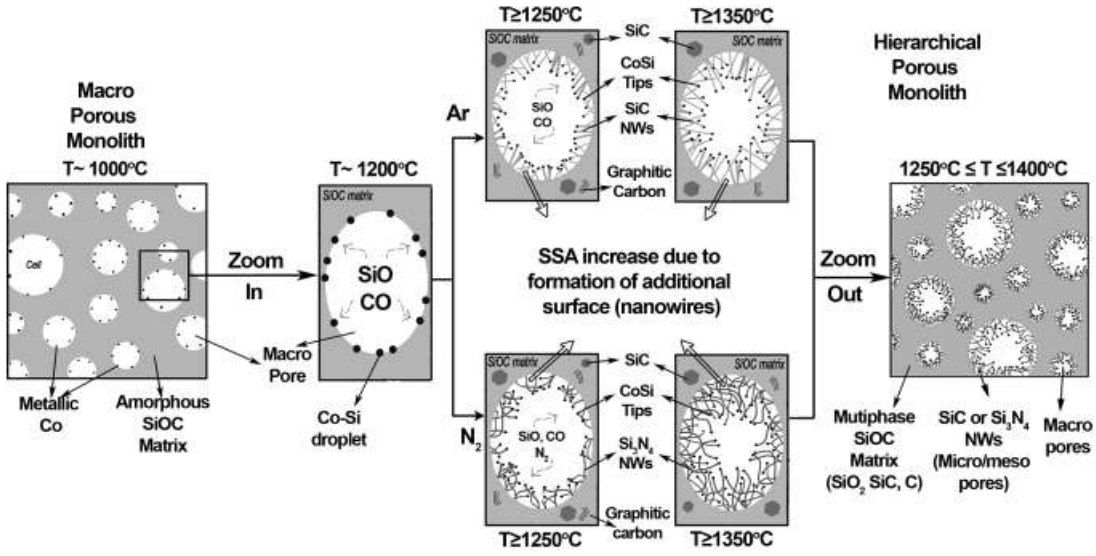

Fig. 12. Schematic representation for the formation of NWs on the cell walls of polymer-derived ceramic foams, with the concurrent enhancement of specific surface area.

processing atmosphere, with N_2-producing single-crystal Si_3N_4 and Ar SiC nanowires. The presence of these nanostructures on the surface of the porous ceramics increased considerably the SSA of the materials (up to $\sim$110 m^2/g), including those produced with $FeCl_2$ as a catalyst, and the observed differences were attributed to the varied nanowire morphology (diameter and assemblage), which depended on the processing conditions and the catalyst type. In particular, increasing the pyrolysis temperature increased the amount and length of the formed nanowires, and the Co catalyst was more effective in the formation of a large amount of thin and bundled nanowires with respect to the Fe catalyst used in a previous study. The proposed one is a simple and effective one-pot method for the fabrication of ceramic components with hierarchical porosity and high SSA.

Acknowledgments

P. C. and C. V. gratefully acknowledge the support of the European Community's Sixth Framework Programme through a Marie-Curie Research Training Network ("PolyCerNet" MRTN-CT-019601). The authors are greatly indebted to Prof. M. Meneghetti of the University of Padova (Dipartimento di Scienze Chimiche) for the use of Raman equipment. This paper is dedicated to the memory of Prof. J. Woltersdorf, who passed away on March 9, 2010.

References

[1]F. Schüth, K. S. W. Sing, and J. Weitkamp, *Handbook of Porous Solids*. Wiley-VCH Verlag GmbH, Weinheim, Germany, 2002, 3191pp.

[2]M. V. Twigg and J. T. Richardson, "Fundamentals and Applications of Structured Ceramic Foam Catalysts," *Ind. Eng. Chem. Res.*, **46** [12] 4166–77 (2007).

[3]S. R. Federman, V. C. Costa, D. C. L. Vasconcelos, and W. L. Vasconcelos, "Sol–Gel SiO_2–CaO–P_2O_5 Biofilm with Surface Engineered for Medical Application," *Mater. Res.*, **10**, 177–81 (2007).

[4]E. Vanhaecke, S. Ivanova, A. Deneuve, O. Ersen, D. Edouard, G. Wine, P. Nguyen, C. Pham, and C. Pham-Huu, "1D SiC Decoration of SiC Macroscopic Shapes for Filtration Devices," *J. Mater. Chem.*, **18** [39] 4654–62 (2008).

[5]E. Garcia-Bordeje, I. Kvande, D. Chen, and M. Ronning, "Carbon Nanofibers Uniformly Grown on y-Alumina Washcoated Cordierite Monoliths," *Adv. Mater.*, **18** [12] 1589–92 (2006).

[6]N. A. Jarrah, J. G. van Ommen, and L. Lefferts, "Development of Monolith with a Carbon–Nanofiber–Washcoat as a Structured Catalyst Support in Liquid Phase," *Catal. Today*, **79–80**, 29–33 (2003).

[7]N. A. Jarrah, J. G. van Ommen, and L. Lefferts, "Growing a Carbon Nano-Fiber Layer on a Monolith Support; Effect of Nickel Loading and Growth Conditions," *J. Mater. Chem.*, **14** [10] 1590–7 (2004).

[8]E. Garcia-Bordeje, I. Kvande, D. Chen, and M. Ronning, "Synthesis of Composite Materials of Carbon Nanofibres and Ceramic Monoliths with Uniform and Tuneable Nanofibre Layer Thickness," *Carbon*, **45** [9] 1828–38 (2007).

[9]K. M. de Lathouder, T. Marques Fló, F. Kapteijn, and J. A. Moulijn, "A Novel Structured Bioreactor: Development of a Monolithic Stirrer Reactor with Immobilized Lipase," *Catal. Today*, **105** [3–4] 443–7 (2005).

[10]K. M. de Lathouder, D. Lozano-Castelló, A. Linares-Solano, F. Kapteijn, and J. A. Moulijn, "Carbon Coated Monoliths as Support Material for a Lactase from *Aspergillus oryzae*: Characterization and Design of the Carbon Carriers," *Carbon*, **44** [14] 3053–63 (2006).

[11]M. A. Ulla, A. Valera, T. Ubieto, N. Latorre, E. Romeo, V. G. Milt, and A. Monzón, "Carbon Nanofiber Growth Onto a Cordierite Monolith Coated with Co-Mordenite," *Catal. Today*, **133–135**, 7–12 (2008).

[12]P. W. A. M. Wenmakers, J. v. d. Schaaf, B. F. M. Kuster, and J. C. Schouten, "'Hairy Foam': Carbon Nanofibers Grown on Solid Carbon Foam. A Fully Accessible, High Surface Area, Graphitic Catalyst Support," *J. Mater. Chem.*, **18** [21] 2426–36 (2008).

[13]C. Pham-Huu and M.-J. Ledoux, "Carbon Nanomaterials with Controlled Macroscopic Shapes as New Catalytic Materials," *Top. Catal.*, **40** [1] 49–63 (2006).

[14]B. Gong, R. Wang, B. Lin, F. Xie, X. Yu, and K. Wei, "Preparation of Carbon Nanotubes (CNTs)-Cordierite Monoliths by Catalytic Chemical Vapor Deposition as Catalyst Supports for Ammonia Synthesis," *Catal. Lett.*, **122** [3] 287–94 (2008).

[15]J. Wang, R. Wang, X. Yu, J. Lin, F. Xie, and K. Wei, "Preparation and Characterization of Carbon Nanotubes-Coated Cordierite for Catalyst Supports," *J. Nat. Gas Chem.*, **15** [3] 211–6 (2006).

[16]S. Rul, C. Laurent, A. Peigney, and A. Rousset, "Carbon Nanotubes Prepared In Situ in a Cellular Ceramic by the Gelcasting–Foam Method," *J. Eur. Ceram. Soc.*, **23** [8] 1233–41 (2003).

[17]V. G. de Resende, E. De Grave, A. Cordier, A. Weibel, A. Peigney, and C. Laurent, "Catalytic Chemical Vapor Deposition Synthesis of Single- and Double-Walled Carbon Nanotubes from α-$(Al_{1-x}Fe_x)_2O_3$ Powders and Self-Supported Foams," *Carbon*, **47** [2] 482–92 (2009).

[18]A. Cordier, E. Flahaut, C. Viazzi, C. Laurent, and A. Peigney, "In Situ CCVD Synthesis of Carbon Nanotubes within a Commercial Ceramic Foam," *J. Mater. Chem.*, **15** [37] 4041–50 (2005).

[19]A. Cordier, F. Rossignol, C. Laurent, T. Chartier, and A. Peigney, "A New Fast Method for Ceramic Foam Impregnation: Application to the CCVD Synthesis of Carbon Nanotubes," *Appl. Catal., A*, **319**, 7–13 (2007).

[20]S. M. Mukhopadhyay, A. Karumuri, and I. T. Barney, "Hierarchical Nanostructures by Nanotube Grafting on Porous Cellular Surfaces," *J. Phys. D: Appl. Phys.*, **42** [19] 195503, 9pp (2009).

[21]D. Edouard, S. Ivanova, M. Lacroix, E. Vanhaecke, C. Pham, and C. Pham-Huu, "Pressure Drop Measurements and Hydrodynamic Model Description of SiC Foam Composites Decorated with SiC Nanofiber," *Catal. Today*, **141** [3–4] 403–8 (2009).

[22]M. G. Segatelli, A. T. N. Pires, and I. V. P. Yoshida, "Synthesis and Structural Characterization of Carbon-Rich SiC_xO_y Derived from a Ni-Containing Hybrid Polymer," *J. Eur. Ceram. Soc.*, **28** [11] 2247–57 (2008).

[23]M. G. Segatelli, E. Radovanovic, M. d. C. Gonçalves, and I. V. P. Yoshida, "Investigation of the Morphological Changes Promoted by Heating of Si–C–O Ceramics Derived from a Phenyl-Rich Hybrid Polymer. Effect of Ni in the Polymeric Precursor," *J. Eur. Ceram. Soc.*, **29** [15] 3279–87 (2009).

[24]S. Zhu, H.-A. Xi, Q. Li, and R. Wang, "In Situ Growth of β-SiC Nanowires in Porous SiC Ceramics," *J. Am. Ceram. Soc.*, **88** [9] 2619–21 (2005).

[25]X. Yao, S. Tan, Z. Huang, S. Dong, and D. Jiang, "Growth Mechanism of β-SiC Nanowires in SiC Reticulated Porous Ceramics," *Ceram. Int.*, **33** [6] 901–4 (2007).

[26]A. Berger, E. Pippel, J. Woltersdorf, M. Scheffler, P. Cromme, and P. Greil, "Nanoprocesses in Polymer-Derived Si–O–C Ceramics: Electronmicroscopic Observations and Reaction Kinetics," *Phys. Status Solidi A*, **202** [12] 2277–86 (2005).

[27]M. Scheffler, P. Greil, A. Berger, E. Pippel, and J. Woltersdorf, "Nickel-Catalyzed In Situ Formation of Carbon Nanotubes and Turbostratic Carbon in Polymer-Derived Ceramics," *Mater. Chem. Phys.*, **84** [1] 131–9 (2004).

[28]C. Vakifahmetoglu, E. Pippel, J. Woltersdorf, and P. Colombo, "Growth of 1D-Nanostructures in Porous Polymer Derived Ceramics by Catalyst-Assisted-Pyrolysis. Part I: Iron Catalyst," *J. Am. Ceram. Soc.*, **93** [4] 959–68 (2010).

[29]V. Bakumov, M. Schwarz, and E. Kroke, "Emulsion Processing of Polymer-Derived Porous Si/C/(O) Ceramic Bodies," *J. Eur. Ceram. Soc.*, **29** [13] 2857–65 (2009).

[30]B.-H. Yoon, C.-S. Park, H.-E. Kim, and Y.-H. Koh, "In Situ Synthesis of Porous Silicon Carbide (SiC) Ceramics Decorated with SiC Nanowires," *J. Am. Ceram. Soc.*, **90** [12] 3759–66 (2007).

[31]C. Vakifahmetoglu and P. Colombo "Porous Polymer Derived Ceramics Decorated with In-situ Grown Nano-structures," pp. 95–103 in *Proceedings of Pac-Rim 8, Advances in Polymer Derived Ceramics and Composites: Ceramic Transactions*, Vol. 213, Edited by P. Colombo and R. Raj. John Wiley & Sons, New York, 2010.

[32]J. Zeschky, T. Höfner, C. Arnold, R. Weißmann, D. Bahloul-Hourlier, M. Scheffler, and P. Greil, "Polysilsesquioxane Derived Ceramic Foams with Gradient Porosity," *Acta Mater.*, **53** [4] 927–37 (2005).

[33]F. Kolár, V. Machovic, and J. Svítilová, "Cobalt-Containing Silicon Oxycarbide Glasses Derived from poly[methyl(phenyl)]siloxane and Cobalt Phthalate," *J. Non-Cryst. Solids*, **352** [26–27] 2892–6 (2006).

[34]ASTM D 3576-98 "Standard Test Method for Cell Size of Rigid Cellular Plastics"; pp. 1–5 in *Annual Book of ASTM Standards*, Vol. 08.02. ASTM D 3576-98, West Conshohocken, PA, 2004.

[35]S. Bourg, B. Boury, and R. J. P. Corriu, "Mixed Si/C/M/O Ceramics from 2,5-Disilahexane/Metal Carbonyl," *J. Mater. Chem.*, **8** [4] 1001–6 (1998).

[36]N. Zhu, Z. Peng, C. Wang, Z. Fu, and H. Miao, "Preparation and Characterization of Bundled One-Dimensional Si_3N_4 Single-Crystalline Nanowires by Catalytic Pyrolysis of a Polymer Precursor," *Solid State Sci.*, **11** [6] 1094–7 (2009).

[37]W. Yang, X. Cheng, H. Wang, Z. Xie, F. Xing, and L. An, "Bundled Silicon Nitride Nanorings," *Cryst. Growth Des.*, **8** [11] 3921–3 (2008).

[38]G. D. Soraru, S. Modena, E. Guadagnino, P. Colombo, J. Egan, and C. Pantano, "Chemical Durability of Silicon Oxycarbide Glasses," *J. Am. Ceram. Soc.*, **85** [6] 1529–36 (2002).

[39]H. J. Kleebe, C. Turquat, and G. D. Soraru, "Phase Separation in an SiCO Glass Studied by Transmission Electron Microscopy and Electron Energy-Loss Spectroscopy," *J. Am. Ceram. Soc.*, **84** [5] 1073–80 (2001).

[40]G. D. Soraru and D. Suttor, "High Temperature Stability of Sol–Gel-Derived SiOC Glasses," *J. Sol–Gel Sci. Technol.*, **14**, 69–74 (1999).

[41]R. Pena-Alonso, G. Mariotto, C. Gervais, F. Babonneau, and G. D. Soraru, "New Insights on the High-Temperature Nanostructure Evolution of SiOC and B-Doped SiBOC Polymer-Derived Glasses," *Chem. Mater.*, **19** [23] 5694–702 (2007).

[42]T. Plachky, Z. Lences, L. Hric, P. Sajgalík, P. Balaz, R. Riedel, and H. J. Kleebe, "Processing and Mechanical Properties of Si_3N_4 Composites Employing Polymer-Derived SiAlOC as Sintering Aid," *J. Eur. Ceram. Soc.*, **30** [3] 759–67 (2010).

[43]A. C. Ferrari and J. Robertson, "Interpretation of Raman Spectra of Disordered and Amorphous Carbon," *Phys. Rev. B*, **61** [20] 14095–9 (2000).

[44]L. G. Cancado, K. Takai, T. Enoki, M. Endo, Y. A. Kim, H. Mizusaki, A. Jorio, L. N. Coelho, R. Magalhaes-Paniago, and M. A. Pimenta, "General Equation for the Determination of the Crystallite Size L[a] of Nanographite by Raman Spectroscopy," *Appl. Phys. Lett.*, **88** [16] 163106–3 (2006).

[45]V. V. Pujar and J. D. Cawley, "Computer Simulations of Diffraction Effects due to Stacking Faults in β-SiC: II, Experimental Verification," *J. Am. Ceram. Soc.*, **84** [11] 2645–51 (2001).

[46]S. Siddiqi and A. Hendry, "The Influence of Iron on the Preparation of Silicon Nitride from Silica," *J. Mater. Sci.*, **20** [9] 3230–8 (1985).

[47]G.-E. Yu, J. Parrick, M. Edirisinghe, D. Finch, and B. Ralph, "Synthesis of Silicon Oxynitride from a Polymeric Precursor," *J. Mater. Sci.*, **28** [15] 4250–4 (1993).

[48]M. Scheffler, T. Gambaryan-Roisman, T. Takahashi, J. Kaschta, H. Muenstedt, P. Buhler, and P. Greil, "Pyrolytic Decomposition of Preceramic Organo

Polysiloxanes"; pp. 239–50 in *Proceedings of Innovative Processing and Synthesis of Ceramics, Glasses, and Composites IV (St. Louis, Missouri), Vol. 115, Ceramic Transactions*, Edited by N. Bansal, and J. P. Singhe. The American Ceramic Society, Westerville, Ohio, 2000.

[49]H. J. Whitlow, Y. Zhang, C. M. Wang, D. E. McCready, T. Zhang, and Y. Wu, "Formation of Cobalt Silicide from Filter Metal Vacuum Arc Deposited Films," *Nucl. Instrum. Methods Phys. Res., Sect. B*, **247** [2] 271–8 (2006).

[50]K. Seo, K. S. K. Varadwaj, P. Mohanty, S. Lee, Y. Jo, M.-H. Jung, J. Kim, and B. Kim, "Magnetic Properties of Single-Crystalline CoSi Nanowires," *Nano Lett.*, **7** [5] 1240–5 (2007).

[51]W. Yang, Z. Xie, J. Li, H. Miao, L. Zhang, and L. An, "Ultra-Long Single-Crystalline α-Si_3N_4 Nanowires: Derived from a Polymeric Precursor," *J. Am. Ceram. Soc.*, **88** [6] 1647–50 (2005).

[52]A. W. Weimer, G. A. Eisman, D. W. Susnitzky, D. R. Beaman, and J. W. McCoy, "Mechanism and Kinetics of the Carbothermal Nitridation Synthesis of α-Silicon Nitride," *J. Am. Ceram. Soc.*, **80** [11] 2853–63 (1997).

[53]C. R. Blanchard and S. T. Schwab, "X-Ray Diffraction Analysis of the Pyrolytic Conversion of Perhydropolysilazane into Silicon Nitride," *J. Am. Ceram. Soc.*, **77** [7] 1729–39 (1994).

[54]Y. Qu, J. D. Carter, and T. Guo, "Silica Nanocoils," *J. Phys. Chem. B*, **110** [16] 8296–301 (2006).

[55]Q. Wei, E. Pippel, J. Woltersdorf, M. Scheffler, and P. Greil, "Interfacial SiC Formation in Polysiloxane-Derived Si–O–C Ceramics," *Mater. Chem. Phys.*, **73** [2–3] 281–9 (2002).

[56]G. Yang, R. Wu, J. Chen, Y. Pan, R. Zhai, L. Wu, and L. Jing, "Growth of SiC Nanowires/Nanorods Using a Fe–Si Solution Method," *Nanotechnology*, **18** [15] 155601, 5pp (2007).

[57]B. C. P. Li, J. F. Gerald, and Y. Chen, "Synthesis of Silicon Nitride Nanowires by Ball Milling and Annealing"; pp. 1–3 in *Proceedings of 30th Annual Condensed Matter and Materials Meeting*, Edited by M. Avdeev, and W. Wagga. Australian Institute of Physics, Melbourne, 2006.

[58]P. C. Silva and J. L. Figueiredo, "Production of SiC and Si_3N_4 Whiskers in C+SiO_2 Solid Mixtures," *Mater. Chem. Phys.*, **72** [3] 326–31 (2001).

[59]Z. Peng, N. Zhu, X. Fu, C. Wang, Z. Fu, L. Qi, and H. Miao, "Growth and Mechanism of Network-Like Branched Si_3N_4 Nanostructures," *J. Am. Ceram. Soc.* (2010), doi: 10.1111/j.1551-2916.2010.03737.x.

[60]R. S. Wagner and W. C. Ellis, "Vapor–Liquid–Solid Mechanism of Single Crystal Growth," *Appl. Phys. Lett.*, **4** [5] 89–90 (1964).

[61]S. Esconjauregui, C. M. Whelan, and K. Maex, "Carbon Nanotube Catalysis by Metal Silicide: Resolving Inhibition Versus Growth," *Nanotechnology*, **18**, 015602, 11pp (2007).

[62]W. Yang, H. Miao, Z. Xie, L. Zhang, and L. An, "Synthesis of Silicon Carbide Nanorods by Catalyst-Assisted Pyrolysis of Polymeric Precursor," *Chem. Phys. Lett.*, **383** [5–6] 441–4 (2004).

[63]H. J. Seifert, J. Peng, H. L. Lukas, and F. Aldinger, "Phase Equilibria and Thermal Analysis of Si–C–N Ceramics," *J. Alloys Compd.*, **320** [2] 251–61 (2001).

[64]D. D. Jayaseelan, W. E. Lee, D. Amutharani, S. Zhang, K. Yoshida, and H. Kita, "In Situ Formation of Silicon Carbide Nanofibers on Cordierite Substrates," *J. Am. Ceram. Soc.*, **90** [5] 1603–6 (2007).

[65]W. Zhou, Y. Zhang, X. Niu, and G. Min, "One-Dimensional SiC Nanostructures: Synthesis and Properties"; pp. 17–59 in *One-Dimensional Nanostructures, Lecture Notes in Nanoscale Science and Technology*, Vol. 3, Edited by Z. M. Wang. Springer, London, 2008.

[66]G. Yang, R. Wu, M. Gao, J. Chen, and Y. Pan, "SiC Crystal Growth from Transition Metal Silicide Fluxes," *Cryst. Res. Technol.*, **42** [5] 445–50 (2007).

[67]F. J. Narciso-Romero and F. Rodríguez-Reinoso, "Synthesis of SiC from Rice Husks Catalysed by Iron, Cobalt or Nickel," *J. Mater. Sci.*, **31** [3] 779–84 (1996).

[68]M. Kruk and M. Jaroniec, "Gas Adsorption Characterization of Ordered Organic–Inorganic Nanocomposite Materials," *Chem. Mater.*, **13** [10] 3169–83 (2001).

[69]S. J. Gregg and K. S. W. Sing, *Adsorption, Surface area and Porosity*. Academic Press, London, 1982, 303pp. □